Formation of Poly(dimethylsiloxane) Gels

J. L. Braun and J. E. Mark*

Department of Chemistry, University of Cincinnati, PO Box 210172, Cincinnati, Ohio 45221-0172

B. E. Eichinger

Accelrys, 9685 Scranton Road, San Diego, California 92121-3752

Received September 10, 2001; Revised Manuscript Received April 1, 2002

ABSTRACT: One of the most important reactions used for room temperature vulcanization of elastomers, hydrosilylation, was investigated by end-linking samples of vinyl-terminated poly(dimethylsiloxane) (PDMS) with silanes having number-average functionalities of 3, 4, and 40−50. The reaction was monitored through SiH consumption up to and beyond the gel point via Fourier transform infrared spectroscopy (FTIR). Size exclusion chromatography (SEC) was used to determine the molecular weights of the sol fractions throughout the reaction. Gel samples were swollen in toluene so that the cycle rank (the proportion of useful intramolecular bonds) could be estimated. The experimental results were compared to results from simulations generated by Accelrys' polymer modeling software. The simulations were also used to predict fractions of loop and dangling chain defects in the gel and distributions of cycle ranks in the sol molecules. The success of this study should encourage extension to other systems, particularly the commercially important polyurethanes.

Introduction

The primary purpose of this study was to examine the effects of the functionality of an end-linking agent on the gelation it produces upon reaction with end-functionalized polymer chains. The resulting materials are elastomers of considerable commercial importance. Experimental data were collected to support computer simulations. FTIR and SEC data were collected throughout the various reactions so that sol molecular weight could be determined as a function of reaction extent. Swelling experiments were also performed in order to obtain estimates of cycle rank as a function of reaction extent for postgelation samples. The fraction of intramolecular bonds for the entire reaction mixture and the number-average molecular weight of the reaction components at the gel point were not directly measurable by experiment, so estimates were made from other experimental results using the formulas presented in the following sections.

Estimated Gel Point Number-Average Molecular Weight. Gelation is a consequence of intermolecular bond formation. Consider the end-linker/polymer system $A_f + B_2$, where the subscripts denote the functionalities of the molecules. According to Flory−Stockmayer (FS) theory,[1]

$$p_{gp} = \frac{1}{\sqrt{r(f_w - 1)}} \tag{1}$$

where p_{gp} is the extent of reaction of A groups at the gel point, r is the initial ratio of A groups to B groups, and f_w is the weight-average value of f. FS theory describes intermolecular reactions fairly well, provided unequal reactivities of like functional groups or diffusion effects are not prevalent. Unfortunately, FS theory does not account for intramolecular reactions; not surprisingly, experimental values of p_{gp} tend to be higher[2,3] than predicted because some reactions form cyclics.

Under the principle assumption of FS theory, namely, that no intramolecular reactions occur, the total number of molecules in the reaction mixture is simply determined by bond formation; every time an intermolecular bond forms, the number of molecules in the solution decreases by one. Consequently, N_{gp}, the number of molecules present at the gel point, can be related to eq 1 by[4]

$$p_{gp} = \frac{N_0 - N_{gp}}{N_{A0}} \tag{2}$$

where N_0 is the number of molecules present initially and N_{A0} is the number of A groups present initially. The quantity N_0 is simply the sum of N_{ch}, the number of molecules of polymer chains present initially, and N_{el}, the number of molecules of end-linker initially present,

$$N_0 = N_{ch} + N_{el} \tag{3}$$

Similarly, N_{ch} and N_{el} can be expressed respectively as

$$N_{ch} = \frac{N_{B0}}{2} = \frac{N_{A0}}{2r} \tag{4}$$

$$N_{el} = \frac{N_{A0}}{f_n} \tag{5}$$

where f_n is the number-average value of f. Equations 1−5 can be combined and rearranged to give

$$N_{gp} = N_{A0}\left[\frac{1}{2r} + \frac{1}{f_n} - \frac{1}{\sqrt{r(f_w - 1)}}\right] \tag{6}$$

The number-average molecular weight at the gel point, $\langle M_n \rangle_{gp}$, can be calculated by dividing m, the mass of the solution components, by N_{gp}/N_{Avo} to yield

$$\langle M_n \rangle_{gp} = \frac{m}{N_{gp}/N_{Avo}} \tag{7}$$

where N_{Avo} is Avogadro's number. The mass m can be

10.1021/ma0116046 CCC: $22.00
Published on Web 05/17/2002

calculated from the initial masses of end-linker and polymer, m_{el} and m_{ch}, respectively, as

$$m = m_{el} + m_{ch} = \frac{N_{el}}{N_{Avo}}M_{el} + \frac{N_{ch}}{N_{Avo}}\langle M_n\rangle_{ch} \qquad (8)$$

The quantities M_{el} and $\langle M_n\rangle_{ch}$ refer respectively to the molecular weight of the end-linker and the number-average molecular weight of the polymer chains initially present. Equations 4−6 and 8 can be substituted into eq 7 to produce an expression for $\langle M_n\rangle_{gp}$ in terms of f. Specifically,

$$\langle M_n\rangle_{gp} = \frac{\left(\frac{2r}{f_n}\right)M_{el} + \langle M_n\rangle_{ch}}{1 + 2r\left[\frac{1}{f_n} - \frac{1}{\sqrt{r(f_w - 1)}}\right]} \qquad (9)$$

Estimated Fraction of Intramolecular Bonds for the Entire Reaction Mixture. Experimental measurements of reaction extent account for both inter- and intramolecular bond formation. The consumption of group A may be described by

$$p = \frac{N_b}{N_{A0}} \qquad (10)$$

where p is the reaction extent. The quantity N_b is the number of bonds formed. Another useful relation between the stoichiometric variables is

$$r = \frac{N_{A0}}{N_{B0}} = \frac{f_n N_{el}}{2N_{ch}} \qquad (11)$$

The total number of molecules in the solution is N, which can be expressed in terms of N_{ch}, N_{el}, N_b, and N_{cyc}, the latter being the number of intramolecular bonds formed, by the simple, exact relation[5]

$$N = N_{ch} + N_{el} - N_b + N_{cyc} \qquad (12)$$

Equations 10−12 can now be combined and rearranged to produce an expression for θ, the fraction of chain ends which form intramolecular bonds, as

$$\theta \equiv \frac{N_{cyc}}{2N_{ch}} = \frac{1}{2}\left(\frac{N}{N_{ch}} - 1\right) + r\left(p - \frac{1}{f_n}\right) \qquad (13)$$

Equation 13 is a variation of an expression for N_r, the number fraction of ring structures, previously published by Stepto (i.e., N_{cyc}/N, in the terminology of this paper).[5] The ratio N/N_{ch} may be determined from experimental measurements of X_{gel}, the gel mass fraction, and $\langle M_n\rangle_{sol}$, the number-average molecular weight of the sol. X_{gel} can be expressed as follows:

$$1 - X_{gel} = X_{sol} = \frac{m_{sol}}{m} = \frac{N_{sol}\langle M_n\rangle_{sol}}{N_{el}M_{el} + N_{ch}\langle M_n\rangle_{ch}} \qquad (14)$$

where m_{sol} is the mass of the sol components, m is the total mass of the reaction components, and N_{sol} is the number of molecules in the sol. If the gel component is defined as the largest molecule in the reaction mixture, then $N = N_{sol} + 1 \approx N_{sol}$, and eq 14 can be solved for N/N_{ch}, with the result

$$\frac{N}{N_{ch}} = \frac{(1 - X_{gel})\left[\left(\frac{2r}{f_n}\right)M_{el} + \langle M_n\rangle_{ch}\right]}{\langle M_n\rangle_{sol}} \qquad (15)$$

Calculation of Cycle Rank. The cycle rank, ξ, in a "perfect" network is related to the molecular weight between network junctions, M_c, as follows:[6]

$$\frac{\xi}{V^0} = \left(1 - \frac{2}{\phi}\right)\left(\frac{\rho}{M_c}\right) \qquad (16)$$

where V^0 is the network volume at formation, ϕ is the number of chains which meet at a network junction, and ρ is the network density at formation. This equation for the elastic modulus of a phantom network is used to interpret our results because phantom network behavior provides a better approximation to the mechanical behavior of swollen networks than does the affine model.[6] Furthermore, it can be shown that[6]

$$M_c = -\frac{\rho\left(1 - \frac{2}{\phi}\right)V_1\left(\frac{\nu_2}{\nu_{2c}}\right)^{1/3}}{\ln(1 - \nu_2) + \nu_2 + \chi{\nu_2}^2} \qquad (17)$$

where V_1 is the molar volume of solvent, ν_2 is the volume fraction of polymer in the swollen sample, ν_{2c} is the volume fraction of polymer during network formation, and χ is the polymer/solvent interaction parameter. Equations 16 and 17 may be combined to eliminate the dependence on ϕ to yield

$$\frac{\xi}{V^0} = -\left(\frac{\nu_{2c}}{\nu_2}\right)^{1/3}\left[\frac{\ln(1 - \nu_2) + \nu_2 + \chi{\nu_2}^2}{V_1}\right] \qquad (18)$$

which provides an unambiguous measure of cycle rank given the validity of Flory−Rehner theory.

Computer Simulations. As stated previously, FS theory[1,7−15] accounts for intermolecular reactions very well but completely neglects cyclization. Gordon−Dušek cascade theory,[16−23] Stepto kinetic theory,[24−26] and Miller−Macosko theory[27−31] are more recent methods which are related to Flory−Stockmayer theory; the first two allow for the formation of some types of cyclics. Percolation theory[32−38] includes all possible cyclization reactions, but it focuses on structureless chains and thus does not distinguish between different chemical polymers or end-linking agents with the same functionality (e.g., PDMS vs polyurethanes or trialkoxysilanes vs triisocyanates). Stepto and Taylor[39] have developed a Monte Carlo algorithm which allows for all possible cyclizations; however, results have only been given for complete reaction.

Accelrys' polymer modeling software calculates properties related to gelation using an algorithm developed by Leung and Eichinger.[40−42] The chemical structures and physical properties of the reactants are required input, and the output includes extents of reaction, average molecular weights for the sol and network, gel and sol weight fractions, and cycle rank. In the Monte Carlo procedure for network formation, polymer and end-linker are randomly distributed throughout the reaction volume. One functionality of each molecule is assigned Cartesian coordinates via a uniform random number generator. In the case of the rigid end-linkers, the coordinates for the remaining functionalities are determined by orienting the molecules randomly; for

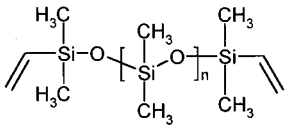

polydimethylsiloxane (PDMS)

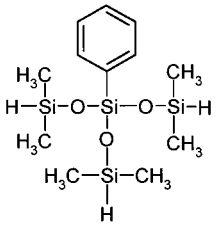

phenyltris(dimethylsiloxy)silane

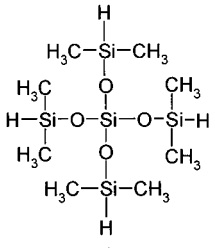

tetrakis(dimethylsiloxy)silane

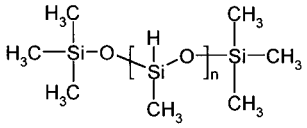

polymethylhydrosiloxane (PMHS)

Figure 1. Reactants. PDMS was end-linked with phenyltris(dimethylsiloxy)silane, tetrakis(dimethylsiloxy)silane, and PMHS.

polymers, one has the choice of using either a Gaussian distribution or RIS generated configurations. If the distances between reactive groups are large, the Gaussian approximation is adequate; if they are short, sampling from RIS configurations will more accurately represent the correlations between reactive groups. The coordinates of the reactive groups do not change as the reaction proceeds, and bond formation is effected by the use of "capture spheres."[40−43] A capture sphere represents the average volume through which a reactive site would diffuse in a unit of time. The reaction is controlled by allowing bond formation between polymer and end-linker reactive sites when the distance between them is within the capture radius. The radius of the capture sphere is incrementally increased to allow the reaction to proceed to completion. The reaction stops when the volume of the capture sphere is equal to the volume of the reaction container. The gel point extent of reaction is defined as an average of two bounds. The lower bound is located by the extremum in the number-average molecular weight of all molecules in the system except for the largest (the incipient gel). The upper bound is the point at which the total average molecular weight of the reaction mixture has a maximum slope.

Experimental Section

Materials. Figure 1 shows the structures of the polymer and end-linkers which were used in the gelation reactions. The number- and weight-average molecular weights of PMHS (Gelest product HMS-991) and vinyl-terminated PDMS (Gelest product DMS-V21) were determined by size exclusion chromatography (SEC); these values are listed in Table 1. The Mark−Houwink constants for PMHS were determined by SEC and viscometry of HMS-991 fractions;[44] constants for PDMS were taken from the literature.[45] The number-average molecular weights of PDMS and PMHS were confirmed respectively by titration with mercuric acetate[46] and mercuric chloride.[47]

Each polymer was refluxed with an equal volume of toluene for 1 h, and then the resulting solutions were distilled in order to remove the toluene and toluene/water azeotrope. PMHS was fractionated using the nonsolvent/solvent pair MeOH/CCl_4 in order to remove cyclics and other polysiloxanes ("silicones") of low molecular weight. The PMHS fraction with $\langle M_n \rangle \sim 3000$ was immediately used in the hydrosilylation reaction in order to avoid significant alcoholysis due to the presence of residual MeOH.[48]

Newly purchased phenyltris(dimethylsiloxy)silane, tetrakis(dimethylsiloxy)silane, and Karstedt's catalyst (Gelest products SIP6826.0, SIT7278.0, and SIP6830.0, respectively) were used as provided by the manufacturer. Dimethyl maleate catalyst inhibitor and the cyclohexane which was used as reaction diluent were dried over molecular sieves overnight and then filtered.

Vinyl-terminated PDMS was end-linked with multifunctional silanes using Karstedt's catalyst, which does not cause unwanted side reactions.[49] The $f = 3$ and $f = 4$ cases were diluted with cyclohexane in order to lower the viscosity during the early stages of the reactions; diluent was not used in the $40 < f_n < 50$ case because it caused poor gel quality.

Procedure for Gels Made with Tri- or Tetrafunctional End-Linkers. 150 μL of dimethyl maleate and 100 mL of cyclohexane were combined and then dried over molecular sieves overnight with continuous stirring. 60 mL of filtered dimethyl maleate/cyclohexane solution, cross-linker [3.2 mL of phenyltris(dimethylsiloxy)silane, or 2.5 mL of tetrakis(dimethylsiloxy)silane] and 90 mL of PDMS were stirred together continuously for 30 min; the resulting mixture had the desired 1:1 ratio of vinyl-to-silicon hydride groups. N_2 was bubbled through the polymer/cross-linker solution for 20 min, and then the reaction vessel was sealed off in order to minimize exposure to O_2 and atmospheric moisture. 250 μL of ∼1:9 catalyst/dimethyl maleate/cyclohexane solution was then introduced via syringe. The reaction was allowed to proceed at room temperature under an N_2 atmosphere, with continuous stirring until the gel point, which was defined as the time when the reaction mixture first begins to climb the stirrer shaft.[5]

Table 1. Simulation Input Parameters

	PDMS + phenyltris(dimethylsiloxy)silane	PDMS + tetrakis(dimethylsiloxy)silane	PDMS + PMHS
reaction vol (Å^3)	1×10^9	1×10^9	2×10^9
no. of PDMS molecules	53459	53686	181045
no. of end-linker molecules	35776	26737	8029
no. of systems averaged	5	5	1
no. of capture radii	123	123	53
PDMS $\langle M_n \rangle$	6420	6420	6420
PDMS $\langle M_w \rangle$	12635	12635	12635
PDMS density (g/mL)	0.97	0.97	0.97
PDMS characteristic ratio	6.4	6.4	6.4
end-linker functionality	3	4	$f_n \sim 45$
end-linker $\langle M_n \rangle$	330.684	328.742	2900
end-linker $\langle M_w \rangle$	330.684	328.742	11200
end-linker density (g/mL)	0.94	0.89	0.98
end-linker characteristic ratio			6.4
vol fraction of diluent	0.39	0.39	0.00

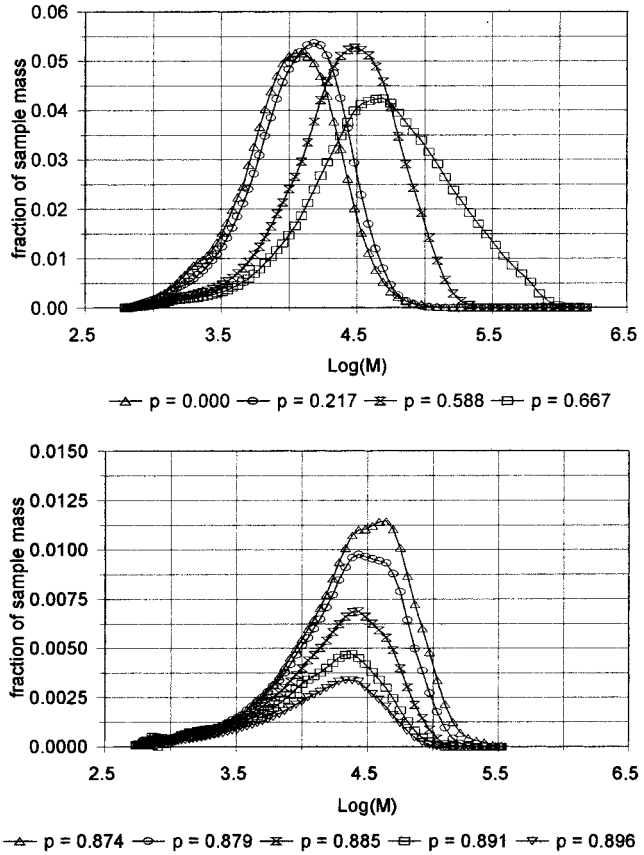

Figure 2. Molecular weight distributions for PDMS/phenyltris(dimethylsiloxy)silane. Part A (top) shows results for a pregelation reaction mixture, and part B (bottom) for postgelation sol results, for this trifunctional case.

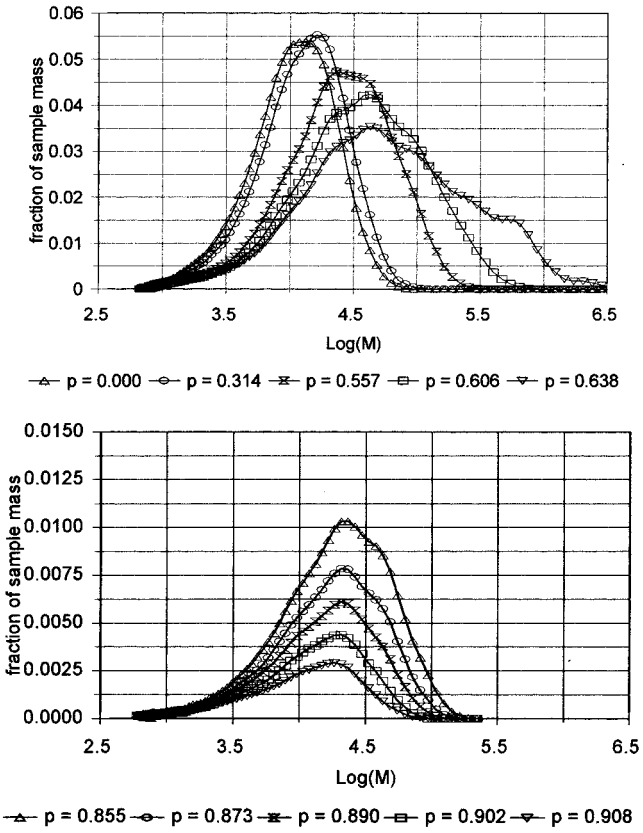

Figure 3. Molecular weight distributions for PDMS/tetrakis(dimethylsiloxy)silane. Part A (top) shows results for a pregelation reaction mixture and part B (bottom) for postgelation sol results, for this tetrafunctional case.

Prior to the gel point, samples of the reaction mixture were periodically removed via syringe and diluted 1:9 with CCl_4 for FTIR analysis. Specifically, the disappearance of the Si−H peak at ∼2100 cm^{-1} was monitored.[50] Samples were also deposited on aluminum foil and allowed to gel. After the gel point, the film made from the last sample collected was peeled from the foil so that it could be monitored periodically via FTIR. The film made from the last pregelation sample was used because it was more thoroughly mixed than the others and, consequently, was more representative of the postgelation reaction mixture.

Prior to the gel point, 250 μL samples were periodically removed from the reaction mixture and quenched with 750 μL portions of triethylamine. The triethylamine was later evaporated from the quenched samples, which were subsequently diluted with 2 mL portions of toluene in preparation for SEC.

After the gel point, ∼0.5 g samples were removed from the solidified reaction mixture and then quenched with 15 mL portions of triethylamine. After 24 h, the triethylamine was decanted, and the extraction procedure was repeated three times using toluene instead of triethylamine. After the third toluene extraction, the swollen gels were weighed, dried in a vacuum oven overnight, and then weighed again. The original sample masses and the masses of the toluene-swollen networks were converted to the volume fractions ν_{2c} and ν_2, which were used to calculate ξ/V^0 via eq 18. Since χ depends on the polymer concentration in the swollen network,[45] the value of χ used in eq 18 was obtained by linear interpolation using $(\nu_2,\chi) = (0.00, 0.45)$ and $(\nu_2,\chi) = (0.20, 0.50)$. The extraction solvents for each sample were combined, evaporated to dryness, and then diluted with 2 mL portions of toluene in preparation for SEC.

Procedure for Gels Made with PMHS. 100 μL of dimethyl maleate and 20 mL of cyclohexane were combined and then dried over molecular sieves overnight with continuous stirring. PDMS and PMHS were combined such that the ratio of vinyl to silicon hydride groups was 1:1 and the total volume was approximately 50 mL. 1 mL of filtered dimethyl maleate/cyclohexane solution was added, and the resulting mixture was stirred continuously for 30 min. Argon was bubbled through the polymer/cross-linker solution for 20 min, and then the reaction vessel was sealed off in order to minimize exposure to O_2 and atmospheric moisture. 250 μL of ∼1:19 Karstedt's catalyst/filtered dimethyl maleate/cyclohexane solution was introduced via syringe. The reaction was allowed to proceed at room temperature under an argon atmosphere, with continuous stirring until the gel point, which was again defined as the time when the reaction mixture first begins to climb the stirrer shaft.[5]

The samples for the postgelation FTIR films were deposited on Scotch transparent mailing tape (Cat. 141), which has a low absorbance in the vicinity of 2100 cm^{-1}. After the gel point, the tape bearing the last film collected was periodically monitored via FTIR. With the exception of $t = 0$, no pregelation samples were collected for FTIR because the early part of the postgelation rate curve was linear and intersected $(t,p) = (0,0)$. Pre- and postgelation samples were collected and processed for SEC and swelling experiments in the same manner used for the $f = 3$ and $f = 4$ cases.

Computer Simulations. Unless stated otherwise, the simulations used the parameters listed in Table 1. Only one large configuration was used for the PDMS/PMHS simulation. Multiple configurations of smaller systems entailed the use of a relatively small number of PMHS molecules, resulting in excessive statistical noise.

Results and Discussion

Sol Number-Average Molecular Weight. Figures 2−4 show the SEC molecular weight distributions of the soluble silicones, both before and after the gel point. In

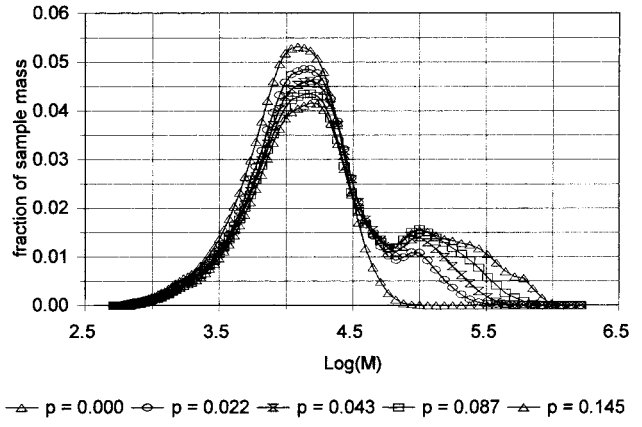

Figure 4. Molecular weight distributions for PDMS/PMHS. Part A (top) shows results for a pregelation reaction mixture and part B (bottom) for postgelation sol results, for this high-functionality case.

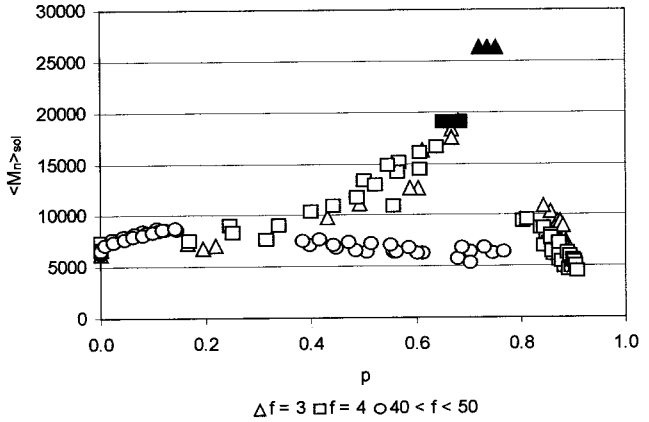

Figure 5. Sol number-average molecular weight as a function of reaction extent. Filled symbols represent $\langle M_n \rangle_{gp}$, as calculated from eq 9.

Figures 2a and 3a, the unreacted PDMS peak has all but disappeared for extents of reaction near the gel point; this shows that nearly all of the PDMS chains have reacted at least once by the gel point and that the distribution of molecular weights for the reacted species is very broad for cases in which the end-linker functionality is low. In Figure 4a, the very small populations of high molecular weight species and the persistence of the unreacted PDMS peak show that very few chains are required for gel formation if the end-linker functionality is very high.

Figures 2b, 3b, and 4b indicate that the larger molecules are preferentially removed from the sol after

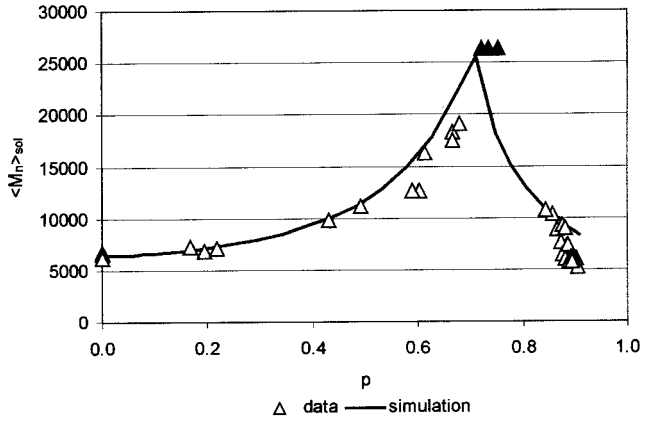

Figure 6. Sol number-average molecular weight as a function of reaction extent for the PDMS/phenyltris(dimethylsiloxy)-silane gels. Data were obtained from multiple trials. Estimates of $\langle M_n \rangle_{gp}$ from eq 9 were plotted at experimentally determined values of p_{gp}.

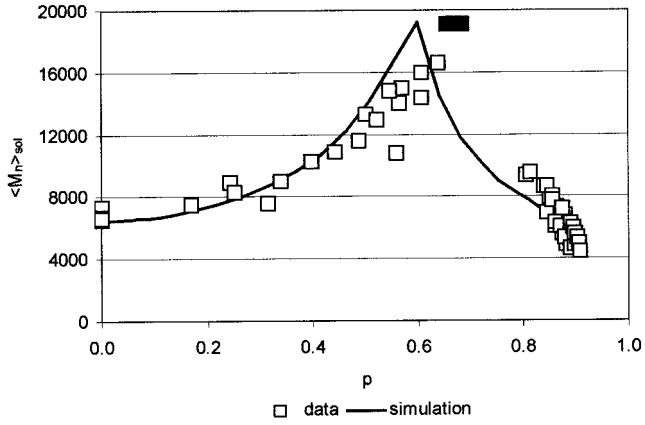

Figure 7. Same representations as in Figure 6, but for the PDMS/tetrakis(dimethylsiloxy)silane gels.

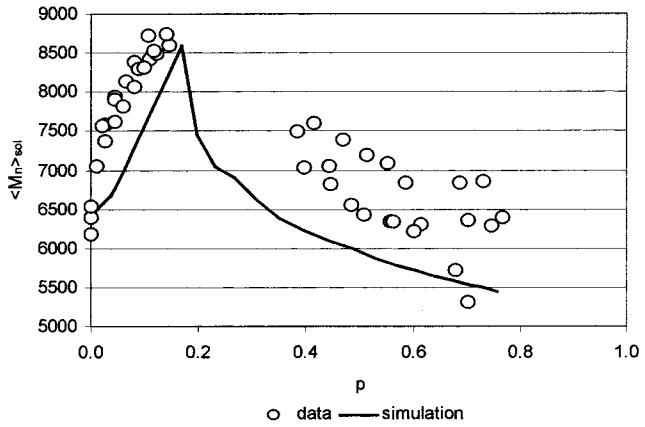

Figure 8. Same representations as in Figure 6, but for the PDMS/PMHS gels.

the gel point. This was to be expected, since the larger the sol molecule, the more groups it would have for attachment to the gel phase. As the reaction extent increases, the distribution of sol molecules becomes more and more like that of unreacted PDMS.

SEC was performed at 35 °C using Waters Ultrastyragel columns and toluene solvent. The only detector for the system was a differential refractometer. Since there was no online viscometer, Mark−Houwink constants were used to correct for compositional differences between PDMS and the polystyrene standards.

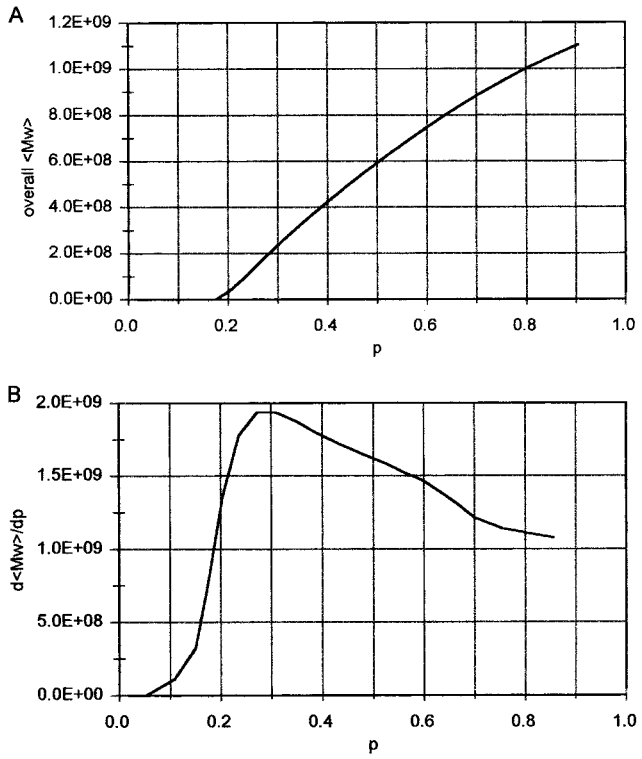

Figure 9. Determination of upper boundary for the PDMS/PMHS gel point extent of reaction. (A) Plot of $\langle M_w \rangle$ vs p for the entire reaction mixture. (B) Differential plot of (A); the upper boundary for the gel point extent of reaction is defined as the maximum value of $d\langle M_w \rangle/dp$.

Unfortunately, this method is not sensitive to the topological differences of the components within a given sample. Consequently, there was some error in calculating the molecular weight distributions because the instrument could not distinguish between straight-chain, cyclic, and branched polymers.

The number-average molecular weights from the SEC data are plotted vs extents of reaction in Figure 5. Experimental limitations preclude direct measurement of $\langle M_n \rangle_{gp}$. Also, collection of data near the gel point is difficult due to high solution viscosity just before gelation and gel fragility immediately afterward. For the $f = 3$ and $f = 4$ cases, the maximum value of $\langle M_n \rangle_{sol}$ was not easily extrapolated from pre- and postgelation data, so values estimated from eq 9 have been included for comparison. Figure 5 shows that the calculated points lie directly along the experimental curves. The results indicate that $\langle M_n \rangle_{gp}$ decreases as f increases.

Figures 6−8 show plots of simulation $\langle M_n \rangle_{sol}$ values vs p for the $f = 3$, $f = 4$ and $40 < f_n < 50$ cases; experimental data and estimated values of $\langle M_n \rangle_{gp}$ have been included for comparison. Both sets of data agree fairly well up to the gel point; afterward, the simulation values are slightly lower, presumably because the software does not account for entanglements and viscosity effects. Estimated and simulation values of $\langle M_n \rangle_{gp}$ are listed in Table 2; the results are fairly close for $f = 3$ and $f = 4$ but not for $40 < f_n < 50$, possibly due to the error involved in characterizing PMHS.

Extents of Reaction. Table 2 also lists gel point extents of reaction from experiment, FS theory (which neglects formation of cyclics), and computer simulations. Experimental gel-point extents of reaction were determined by Lagrange polynomial interpolation of the pre- and postgelation FTIR absorbance vs time curves for the Si−H peak at ∼2100 cm^{-1}. For the simulation results, ranges are listed because upper and lower bounds are determined from molecular weight plots. The lower bound is the extent of reaction p associated with the maximum value of $\langle M_n \rangle_{sol}$, the sol number-average molecular weight, as is shown by Figures 6−8. The upper bound is the value of p for which the plot of $\langle M_w \rangle$ of the reaction mixture vs p has its maximum slope, as is illustrated by parts A and B of Figure 9. The range of gel point p values is usually narrow for end-linking reactions. The broad range seen for the $40 < f_n < 50$ case is a consequence of the structure of PMHS. Since PMHS is itself of considerable length, this system can be viewed as the cross-linking of PMHS by PDMS. The system is therefore more similar to the cross-linking of polydienes with, say, sulfur;[51] however, in our simulations, the number of divalent molecules is very much larger than is typically the case in the cross-linking of polydienes, so there is a dilution effect. PMHS could also introduce some sequences that would act as the short chains in an inadvertently produced bimodal network.[52] In any case, for this system the lower bound seems to be much more representative of the experimentally observed gel point.

Table 2. Variation of Gel Point Data with End-Linker Functionality

end-linker functionality	trial	extent of Si−H consumption at the gel point	$\langle M_n \rangle_{gp}$	last measured extent of Si−H consumption
3	1	0.72		0.90
	2	0.74		0.90
	3	0.75		0.90
	simulation	0.72−0.74	26000	
	FS estimate	0.71	26300	
4	1	0.65		0.87
	2	0.68		0.89
	3	0.66		0.90
	4	0.65		0.91
	simulation	0.60−0.64	19400	
	FS estimate	0.58	19100	
$40 < f_n < 50$	1	0.18		0.77
	2	0.18		0.76
	3	0.15		0.77
	simulation	0.18−0.27	8600	
	FS estimate	0.15	7300	
	extrapolation		8800	

Table 2 shows that the gel point extent of reaction decreases as the end-linker functionality increases. The discrepancies between the FS gel point extents of reaction and the experimental and computed values reflect cyclic formation. The $f = 3$ and $f = 4$ reaction mixtures were 39% diluent by volume; this undoubtedly enhanced cyclization.[2,53,54]

Table 2 also lists the last measured extents of reaction. A reaction was considered to be terminated for all practical purposes when the extent failed to change for 2 consecutive days. These extents are less than 1 because high viscosity and entanglements prevent formation of some bonds. The $40 < f_n < 50$ case has a much lower maximum extent of reaction than the $f = 3$ and $f = 4$ cases because the degree of entanglement increases as f increases. Values are not listed for the simulation results. In the simulations, the reaction always goes to completion because the software does not account for entanglements and high viscosity.

Gel Mass Fraction. Figure 10 shows plots of X_{gel}, the gel mass fraction, vs extent of reaction for both experimental and simulation results. These results are consistent with the results presented in Figures 5−8:

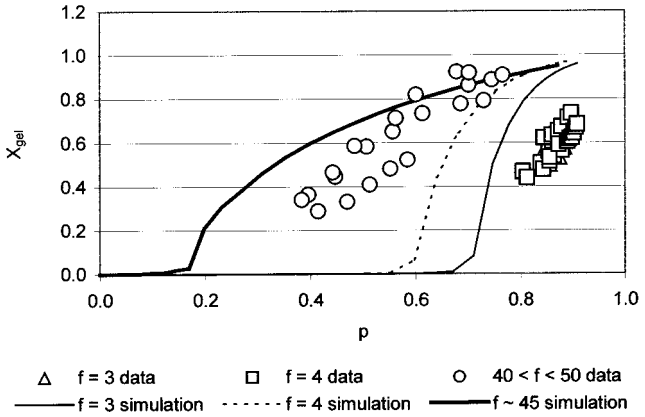

Figure 10. Gel mass fraction as a function of reaction extent.

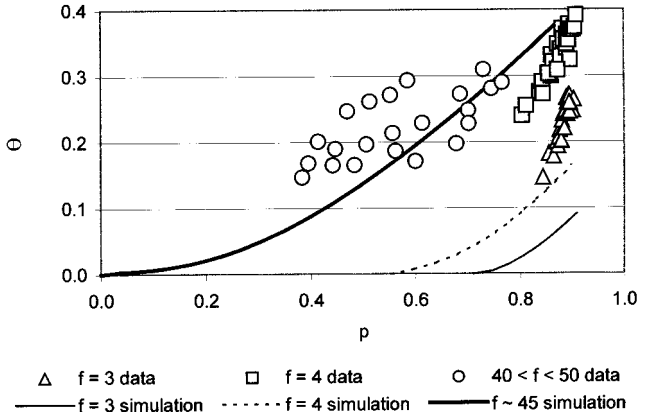

Figure 11. Fraction of intramolecular bonds in the reaction mixture (θ) as a function of reaction extent.

the onset of gelation is inversely related to the end-linker functionality, and the gel mass fraction for a given extent of reaction increases as the end-linker functionality increases. The results presented in Figure 10 should be interpreted with a certain amount of caution, however, since the PDMS/PMHS reaction mixtures were more concentrated than the others were. Dilution increases the number of single-chain loops and decreases the cycle rank and the number of effective chains.

The experimental curves of Figure 10 are shifted to significantly higher extents of reaction than the simulation curves are. The discrepancies could be caused by a systematic error in the estimation of the reaction extents from the FTIR data. They could also be caused by the assumption that all the silane groups on a given end-linker molecule are equally reactive. Consider the case of a trifunctional end-linker. Reaction of one of the silanes introduces a bulky group into the molecule, which can hinder the interactions of the other two silanes with unreacted vinyl groups in their vicinities. Reaction of a second group on the end-linker introduces another obstacle for the remaining unreacted silane. The successively decreasing reactivity of silanes on the same end-linker may retard growth of the gel molecule by favoring reactions on smaller molecules. The discrepancies appear to be less severe for the $f = 3$ case than for the other two; this indicates that steric hindrance is less of a problem for phenyltris(dimethylsiloxy)silane than it is for tetrakis(dimethylsiloxy)silane or PMHS.

Intramolecular Bonds. Figure 11 shows plots of θ, the intramolecular bond fraction of the reaction mixture, vs reaction extent for the $f = 3$, $f = 4$, and $40 < f_n < 50$ cases. For both experimental and simulation values, θ was estimated from X_{gel}, $\langle M_n \rangle_{sol}$, and p using eqs 13 and 15. The simulation curves show the same trends as the data: for any given extent of reaction, the fraction of intramolecular bonds increases as the end-linker functionality increases.

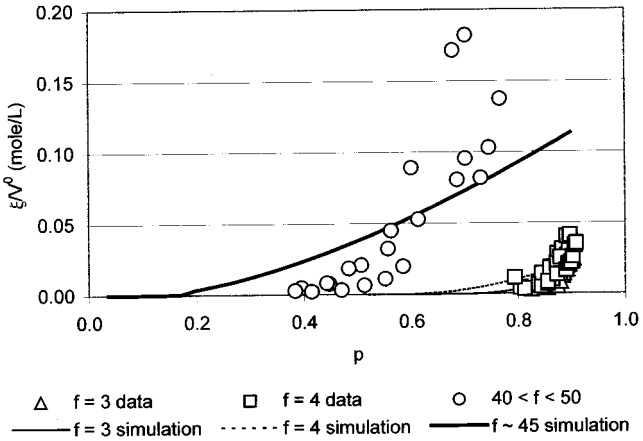

Figure 12. Gel cycle rank (ξ/V^0) as a function of reaction extent.

Figure 12 shows plots of ξ/V^0 vs reaction extent, where ξ is the cycle rank of the network (i.e., the number of mechanically effective intramolecular bonds in the network). The discrepancies between experimental and simulation results may be partly due to the sensitivity of the former to the value of χ used; entanglements may also be a source of error. Nevertheless, the experimental and simulation values show the same trend: for a given extent of reaction, the cycle rank increases as the end-linker functionality increases.

Figures 11 and 12 present different kinds of information concerning intramolecular bonds. The quantity θ accounts for all of the intramolecular bonds within the reaction mixture while ξ/V^0 accounts only for mechanically effective intramolecular bonds in the network. Comparison of Figures 11 and 12 shows that, for any given value of p, the $f = 3$ and $f = 4$ networks have roughly equal quantities of mechanically effective intramolecular bonds, although the $f = 4$ reaction mixture has a greater overall number of intramolecular bonds; this suggests that the $f = 4$ reaction mixture contains more single-chain loops. Single-chain loops are mechanically significant only when they are threaded by polymer chains which are attached by both ends to the network, as illustrated by Figure 13; the probability of this occurrence is low for small loops. Experiments have shown that cyclic siloxanes with degrees of polymerization (dp) below 20 are not trapped at all, while nearly all of those with dp > 250 are threaded.[55] For the PDMS used in this study, the number-average dp = 87, which means that most single-chain loops will not be threaded, although loops with two or more chains very likely will be.

Figure 11 clearly shows that the PDMS/PMHS system formed many more intramolecular bonds for a given extent of reaction than the other two cases did, even though its reaction mixtures were more concentrated. Dilution favors intramolecular bond formation, particularly formation of single-chain loops. Consequently, the $40 < f_n < 50$ results from Figure 12 must be compared to the $f = 3$ and $f = 4$ results with caution, since the lower values of ξ/V^0 for the latter may be partly due to

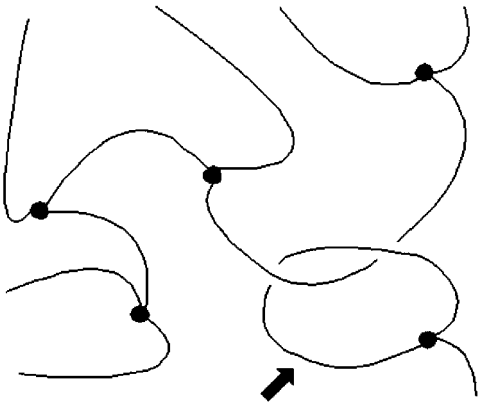

Figure 13. Mechanically effective single-chain loop (lower right-hand corner).

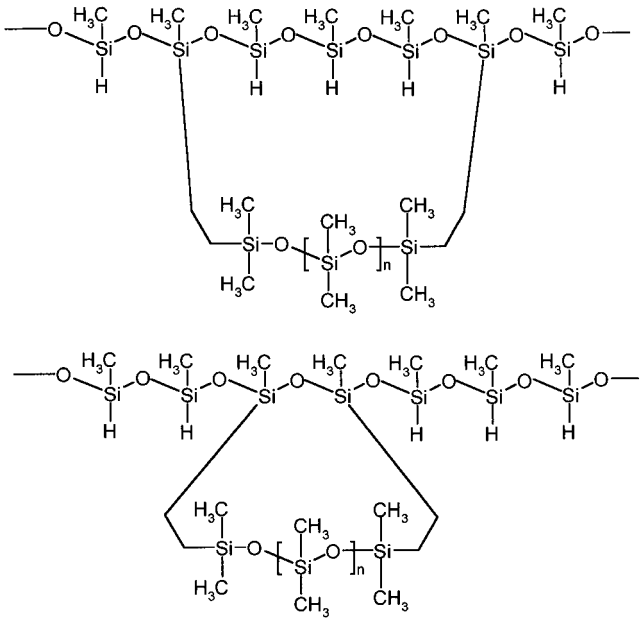

Figure 14. Examples of PDMS/PMHS single-chain loops.

dilution-favored single-chain loop formation at the expense of macrocycles. Macrocycles are more likely to be threaded with other chains, although their mechanical effectiveness is probably lower.[39,56] The PDMS/PMHS situation is further complicated by the variation in size of its single-chain loops, as is illustrated by Figure 14. PMHS molecules vary in length and the distances between silanes on a given PMHS molecule vary; consequently, PDMS/PMHS single-chain loops tend to be larger than those of the $f = 3$ and $f = 4$ reaction mixtures, and the probability of their being threaded is somewhat higher.

Figure 15 shows the increase in the numbers of single-chain loops on the gel with reaction progress, as predicted by the computer simulations. PDMS/PMHS results are not shown due to the difficulty of defining single-chain loops for that case. The $f = 3$ and $f = 4$ results indicate that this type of defect becomes significant after the gel point and, for a given extent of reaction, increases as end-linker functionality increases. Figure 15 probably represents lower boundaries for loop formation, since the software does not account for entanglements and high viscosity, which inhibit molecular motion over long distances and thereby promote loop formation. Entanglements and high viscosity also limit the maximum obtainable reaction extent.

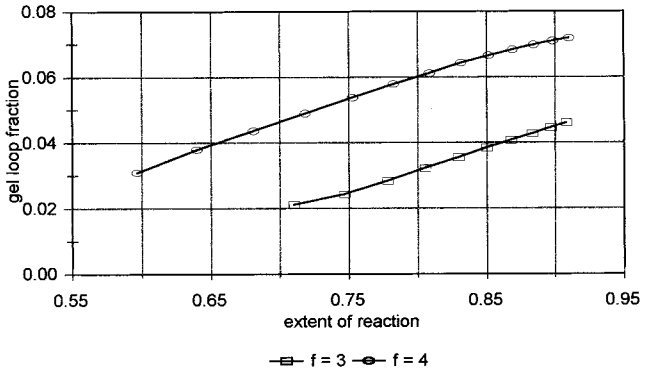

Figure 15. Fraction of gel chains which form loops for the $f = 3$ and $f = 4$ cases, as predicted by computer simulation. Values for PDMS/PMHS are not shown, owing to the difficulty of defining a loop for this case.

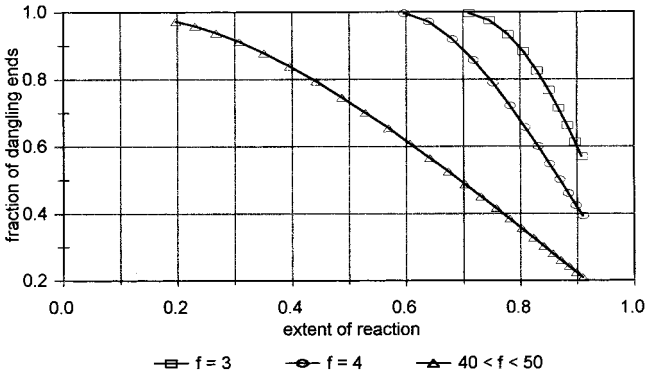

Figure 16. Fraction of gel chains which form dangling ends.

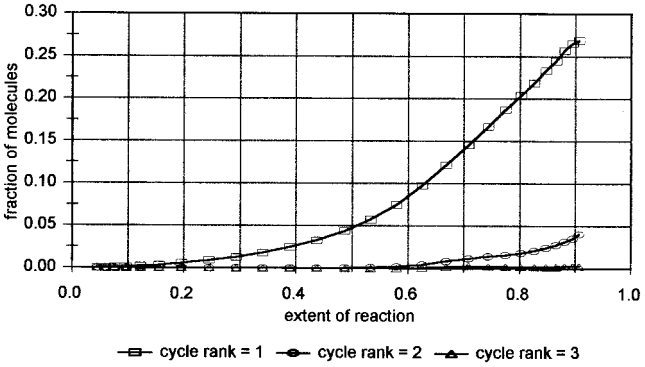

Figure 17. Fractions of sol molecules having $\xi > 0$ for the $f = 3$ case.

Dangling Ends. Figure 16 shows computer predictions of elastically ineffective chains, specifically dangling ends, pendant fragments, and chains that attach pendant fragments to the gel. The numbers of these defects decrease as the reaction progresses because most of them still bear reactive groups. Assuming the reaction could go to completion, the only defects at $p = 1$ would be pendant cyclics and the chains that attach them to the gel.

Figures 17−19 show computer predictions of changes in the cycle ranks of the sol molecules with reaction progress. For any given extent of reaction, the fraction of sol molecules having $\xi > 0$ decreases as f increases. For the $f = 3$ and $f = 4$ cases, the fractions of sol molecules having $\xi > 0$ increases throughout the reaction. For the $40 < f_n < 50$ case, the fraction of sol molecules having $\xi > 0$ reaches a maximum near the gel point and then drops dramatically; this occurs

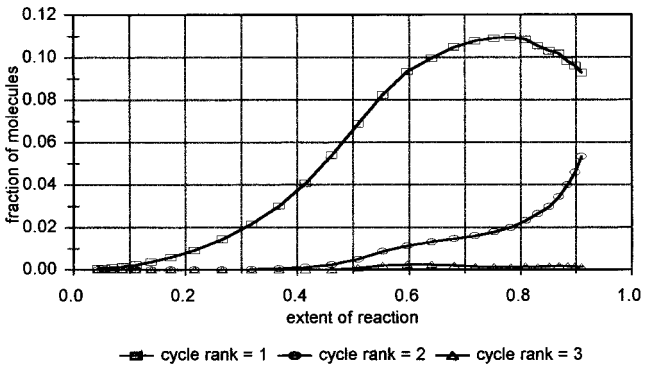

Figure 18. Fractions of sol molecules having $\xi > 0$ for the $f = 4$ case.

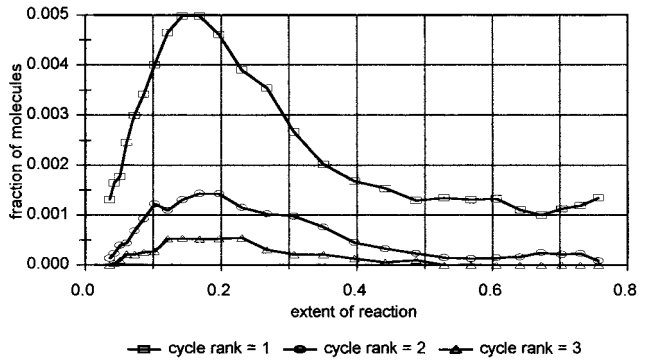

Figure 19. Fractions of sol molecules having $\xi > 0$ for the $f_n \sim 45$ case.

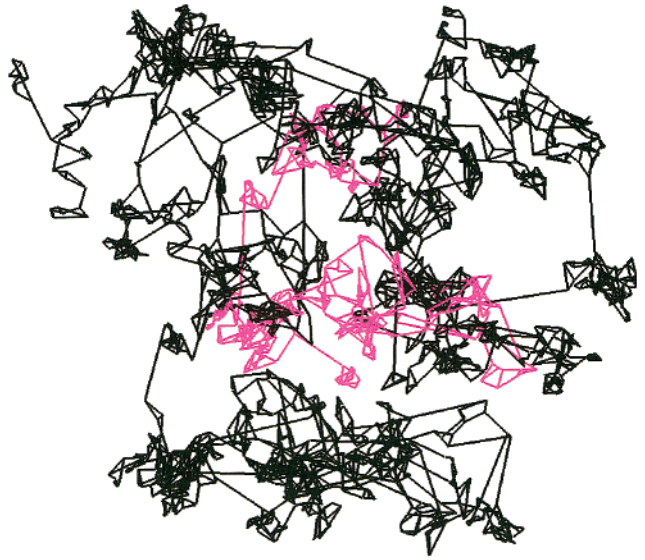

Figure 20. Structure of the largest molecule in the PDMS/PMHS reaction mixture immediately before the gel point (pink structure) and immediately afterward (black structure).

because the many reactive groups on PMHS ensure that it will be rapidly incorporated into the gel, despite the formation of a few intramolecular bonds.

Gel Structure. Figure 20 shows the largest molecule in the PDMS/PMHS reaction mixture just before (pink structure) and immediately after (black structure) the gel point. Only trivalent and higher nodes, together with adjoining chains, are shown; dangling ends have been omitted for purposes of clarity. The figure shows that the network is spatially heterogeneous, with regions of high cross-link density held together tenuously by a few long chains. The heterogeneity decreases as the reaction proceeds because more connecting PDMS chains are added. For the $f = 3$ and $f = 4$ cases, the network is relatively homogeneous near the gel point; because the silane group concentrations are the same as for the $40 < f_n < 50$ case, there are fewer reactive groups per molecule and larger numbers of molecules, so the silane groups can be more evenly distributed.

Conclusions

Experimental gel point extents of reaction fell within or near the ranges predicted by computer simulation. The ranges were narrow for the $f = 3$ and $f = 4$ cases, as is expected for end-linking reactions. However, the range for the $40 < f_n < 50$ case was very broad. With the exception of the upper boundary for the PDMS/PMHS reaction, experimental, estimated, and computed and gel point extents of reaction were in fairly close agreement; this indicates that few cyclics form before the gel point, which supports their neglect in the theory. The simulation results also supported a trend which was observed experimentally: the gel point extent of reaction decreases as the end-linker functionality increases.

Gel point number-average molecular weights from the simulations agreed fairly closely with values estimated from FS theory. The results also indicated another trend: the number-average molecular weight at the gel point decreases as the end-linker functionality increases. Plots of $\langle M_n \rangle_{sol}$ vs p from the simulations were comparable to the experimental data, although some slight discrepancies after the gel point were attributed to entanglements and high viscosity, which are not addressed by the simulations.

For a given extent of reaction, values of X_{gel} predicted by the simulations tended to exceed those seen experimentally. The discrepancies are most likely caused by the assumption that silane groups located on the same end-linker are equally reactive. In reality, the reaction of a given silane with a polymer molecule introduces a bulky group which can interfere with the ability of the end-linker's remaining silanes to react. This is demonstrated by the differing degrees of discrepancy seen in the $f = 3$ and $f = 4$ cases, which have similar end-linkers; since tetrakis(dimethylsiloxy)silane is less abundant but has more silane groups per molecule, these groups are more susceptible to unequal reactivities than the silanes of phenyltris(dimethylsiloxy)silane are.

Gel cycle ranks and θ values calculated from simulation results were consistent with experimental values; these results showed that the tendency to form intramolecular bonds increases as end-linker functionality increases. The computer simulations predicted higher numbers of single-chain loops for the $f = 4$ gel than for the $f = 3$ gel. Comparisons of the sols showed that the fraction of sol molecules with $\xi > 0$ decreases with increasing end-linker functionality.

Similarly useful information could be obtained by carrying out analogous experiments and simulations on other end-linked materials. An example would be the polyurethanes formed in the triisocyanate end-linking of hydroxyl-terminated polymers of various types.

Acknowledgment. It is a pleasure to acknowledge the financial support provided J.E.M. by the National Science Foundation through Grant DMR-0075198 (Polymers Program, Division of Materials Research).

References and Notes

(1) Flory, P. J. *Principles of Polymer Chemistry*; Cornell University Press: Ithaca, NY, 1953; pp 346−353.

(2) Stepto, R. F. T. In *Polymer Networks: Principles of Their Formation, Structure and Properties*; Stepto, R. F. T., Ed.; Blackie Academic and Professional: London, 1998, pp 36−40.
(3) Eichinger, B. E.; Akgiray, O. In *Computer Simulation of Polymers*; Colburn, E. A., Ed.; Longman: Harlow, UK, 1994; pp 271, 291.
(4) Braun, J. L. Ph.D. Thesis in Chemistry, The University of Cincinnati, 2001; pp 54−59.
(5) Stanford, J. L.; Stepto, R. F. T. *Br. Polym. J.* **1977**, *9*, 124.
(6) Erman, B.; Mark, J. E. *Structures and Properties of Rubber-like Networks*; Oxford University Press: Oxford, 1997; pp 57, 66−70, 307−309.
(7) Flory, P. J. *J. Am. Chem. Soc.* **1941**, *63*, 3083.
(8) Flory, P. J. *J. Am. Chem. Soc.* **1941**, *63*, 3091.
(9) Flory, P. J. *J. Am. Chem. Soc.* **1941**, *63*, 3096.
(10) Stockmayer, W. H. *J. Chem. Phys.* **1943**, *11*, 45.
(11) Stockmayer, W. H. *J. Chem. Phys.* **1944**, *12*, 125.
(12) Flory, P. J. *Ind. Eng. Chem.* **1946**, *38*, 417.
(13) Flory, P. J. *Chem. Rev.* **1946**, *39*, 137.
(14) Flory, P. J. *J. Am. Chem. Soc.* **1947**, *69*, 30.
(15) Flory, P. J. *J. Am. Chem. Soc.* **1952**, *74*, 2718.
(16) Gordon, M. *Proc. R. Soc. London A* **1962**, *268*, 240.
(17) Dobson, G. R.; Gordon, M. *J. Chem. Phys.* **1965**, *43*, 705.
(18) Dušek, K.; Gordon, M.; Ross-Murphy, S. B. *Macromolecules* **1978**, *11*, 236.
(19) Dušek, K.; Prins, W. *Adv. Polym. Sci.* **1969**, *6*, 1.
(20) Dušek, K.; Vojta, V. *Br. Polym.* **1977**, *9*, 164.
(21) Mikes, J.; Dušek, K. *Macromolecules* **1982**, *15*, 93.
(22) Dušek, K. *Macromolecules* **1984**, *17*, 716.
(23) Dušek, K.; Spirkova, M.; Havlicek, I. *Macromolecules* **1990**, *23*, 1775.
(24) Ahmad, Z.; Stepto, R. F. T. *Colloid Polym. Sci.* **1980**, *258*, 663.
(25) Stepto, R. F. T. In *Advances in Elastomers and Rubber Elasticity*; Lal, J., Mark, J. E., Eds.; Plenum Press: New York, 1986; p 329.
(26) Stepto, R. F. T. In *Biological and Synthetic Polymer Networks*; Kramer, O., Ed.; Elsevier: London, 1988; Chapter 10, p 153.
(27) Macosko, C. W.; Miller, D. R. *Macromolecules* **1976**, *9*, 199.
(28) Miller, D. R.; Macosko, C. W. *Macromolecules* **1976**, *9*, 206.
(29) Miller, D. R.; Macosko, C. W. *J. Polym. Sci., Polym. Phys.* **1987**, *25*, 2441.
(30) Miller, D. R.; Macosko, C. W. *J. Polym. Sci., Polym. Phys.* **1988**, *26*, 1.
(31) Miller, D. R. *Makromol. Chem., Macromol. Symp.* **1989**, *30*, 57.
(32) Stauffer, D. *Introduction to Percolation Theory*; Taylor & Francis: London, 1985.
(33) Stauffer, D.; Coniglio, A.; Adam, M. *Adv. Polym. Sci.* **1982**, *44*, 103.
(34) Stanley, H. E. *Introduction to Phase Transitions and Critical Phenomena*; Oxford Press: New York, 1971.
(35) Essam, J. W.; Gaunt, D. S.; Gutmann, A. J. *J. Phys. (Paris)* **1978**, *A11*, 1983.
(36) Nakanishi, H.; Stanley, H. E. *Phys. Rev.* **1980**, *B22*, 2466.
(37) Nakanishi, H.; Stanley, H. E. *J. Phys. (Paris)* **1981**, *A14*, 93.
(38) Gawlinski, E. T.; Stanley, H. E. *J. Phys. (Paris)* **1981**, *A14*, L291.
(39) Stepto, R. F. T.; Taylor, D. J. R. In *Wiley Polymer Network Group Review Series*; Stokke, B. T., Elgsaeter, A., Eds.; John Wiley & Sons Ltd.: New York, 1999; Vol. 2, Chapter 8, pp 109−121.
(40) Leung, Y. K.; Eichinger, B. E. *J. Chem. Phys.* **1984**, *80*, 3877.
(41) Leung, Y. K.; Eichinger, B. E. *J. Chem. Phys.* **1984**, *80*, 3885.
(42) *Polymer 4.0.0: Polymer Modeling Software User Guide, Part 1*; Accelrys Publication: San Diego, CA, 1996; pp 7−18.
(43) Shy, L. Y.; Eichinger, B. E. *Br. Polym. J.* **1985**, *17*, 200.
(44) Keqiang, W.; Honghong, H.; Jianfang, S. *J. Liq. Chromatogr. Relat. Technol.* **1998**, *21*, 1457.
(45) Brandrup, J.; Immergut, E. H.; Grulke, E. A. *Polymer Handbook*, 4th ed.; John Wiley & Sons: New York, 1999; pp VII-23, VII-4.
(46) Siggia, S. *Quantitative Organic Analysis*; John Wiley & Sons: New York, 1963; pp 341−348.
(47) Smith, A. L. *The Analytical Chemistry of Silicones*; John Wiley & Sons: New York, 1991; pp 199−201.
(48) Brook, M. A. *Silicon in Organic, Organometallic and Polymer Chemistry*; John Wiley & Sons: New York, 2000; pp 176, 177.
(49) Sargent, J. R.; Weber, *W. P. Polym. Prepr.* **1999**, *40*, 60.
(50) Socrates, G. *Infrared Characteristic Group Frequencies*, 2nd ed.; John Wiley & Sons: New York, 1994; p 190.
(51) Taylor, G. K.; Castner, E. S.; Galiatsatos, V. *J. Chem. Soc., Faraday Trans.* **1995**, 2655.
(52) Mark, J. E. *Rubber Chem. Technol.* **1999**, *72*, 465.
(53) Stepto, R. F. T.; Taylor, D. J. R.; Gottlieb, M. *Polym. Prepr.* **1998**, *39*, 558.
(54) Stepto, R. F. T. In *Silicones and Silicone-Modified Materials*; Clarson, S. J., Fitzgerald, J. J., Owen, M. J., Smith, S. D., Eds.; ACS Symposium Series 729; American Chemical Society: Washington, DC, 2000; Chapter 12, pp 194−203.
(55) Clarson, S. J. In *Cyclic Polymers*; Semlyen, J. A., Ed.; Kluwer Academic Publishers: Dordrecht, 2000; Chapter 5, p 173.
(56) Dutton, S.; Stepto, R. F. T.; Taylor, D. J. R. *Macromol. Symp.* **1997**, *118*, 199.

MA0116046